ChemComm

COMMUNICATION

View Article Online
View Journal | View Issue





Cite this: *Chem. Commun.*, 2021, **57**, 2943

Received 10th January 2021,
Accepted 10th February 2021

DOI: 10.1039/d1cc00156f

rsc.li/chemcomm

# Interfacial cationization to quicken redox-responsive drug release†

Yaxin Zheng,[a] Jie Lei,[a] Qi Li,[a] Xuan Jin,[a] Qingyuan Li[a] and Yang Li *[b]

**Interfacial cationization could greatly increase the redox-responsiveness of disulfide bond-linked lipid-drug nanoassemblies (NAs) due to the generation and concentration of ionized thiols at the alkalized NAs' cationic interface. This strategy could be used to prepare redox-ultrasensitive nanocarriers for efficient intracellular drug delivery.**

The disulfide bond (SS)-containing drug delivery systems (DDSs) have been widely used for the intracellular delivery of various drugs by responding to the high level of glutathione (~2–10 mM) in the cytosol, of which the concentration is around 2 to 3 orders higher than that in the extracellular fluids (approximately 2–20 μM).[1–4] Glutathione is readily able to cleave the SS *via* a thiol–SS exchange reaction, thus accelerating drug release due to the direct nanocarrier destruction or the rapid hydrolysis of adjacent esters linked to the parent drugs. The introduction of SS in the DDSs is always associated with improved antitumor activity, which is mainly ascribed to the selective release of active drugs at the tumor site.[5–7] Therefore, the design of sensitive redox-responsive DDSs has received great interest in the past few decades.

A variety of redox-activatable DDSs with SS linkages have been developed with promising antitumor efficiency.[8–11] Once internalized into cells, the active drugs are expected to be released as soon as possible to exert therapeutic effects. Therefore, a great many efforts have been made to enhance the redox-responsiveness of DDSs.[12,13] The strategies to increase the redox responsiveness of DDSs are mainly based on the chemical modification of the SS-containing linker, such as chemical optimizations of the position of SS in the linkage and the type of adjacent linkers (*e.g.* ester, amide, carbamate and carbonate). For example, combining SS with carbonate is reported to be more effective to trigger drug release due to its more effective self-immolation mechanism upon reduction.[14] The position of SS in the carbon chain linkage also exerts significant effects on their redox responsiveness, which can further influence the drug release rate and *in vivo* antitumor efficacy of SS-containing DDS.[15] On the other hand, the steric hindrance and electrostatic microenvironment around SS linkers can significantly influence the redox-responsiveness of SS-containing linkers.[16,17] These chemical methods are effective to increase the redox-responsiveness of SS linkers, but may also change their chemical stability to induce the premature drug release.[16] To address this, we developed a novel strategy to increase the redox-responsiveness of SS-containing DDSs, without the need to change the chemical structure of the linkers. This strategy was associated with the interfacial cationization of nanocarriers, which could modulate redox-responsiveness as high as 3 orders of magnitude due to greatly the changed pH at the interfaces.

As a proof of concept, self-assembling redox-responsive nanoassemblies (NAs) formed by SS-linked lipophilic prodrugs were used as model DDSs. For this purpose, camptothecin (CPT) and curcumin (CUR) were chosen as model drugs, which were then conjugated with oleic acid (OA) *via* the disulfanylethyl carbonate (ETCSS) linker to obtain the corresponding CPT-SS-2OA and CUR-SS-2OA. Their chemical structures, $^1$H-NMR and mass spectra (MS) are shown in Fig. 1A and Fig. S1 (ESI†), respectively. The PEGylated NAs consisting of CPT-SS-2OA and CUR-SS-2OA (1/2, mole/mole) (CPT/CUR-NAs) were prepared by dispersing their ethanol solutions (containing 10% DON-PEG$_{2000}$, as a neutral stabilizing agent, $^1$H-NMR and MS shown in Fig. S2, ESI†) in water under vigorous stirring. To prepare the cationic CPT/CUR-NAs (+CPT/CUR-NAs), the cationic lipid of DOTAP (10%, by weight) was co-assembled with lipophilic prodrugs using the same preparation procedure. Dynamic light scattering revealed that both unmodified and cationic CPT/CUR-NAs had similar average

[a] *School of Pharmacy, Key Laboratory of Sichuan Province for Specific Structure of Small Molecule Drugs, Chengdu Medical College, Chengdu, China*
[b] *Department of Pharmaceutics, College of Pharmacy, Chongqing Medical University, Chongqing 400016, P. R. China. E-mail: beyond20061330@163.com*

† Electronic supplementary information (ESI) available: Experimental section, $^1$H-NMR and MS of CPT-2S-2OA, CUR-2S-2OA, DON-PEG$_{2000}$ and DON-COOH, cellular uptake, size distributions and fluorescence response of CPT/CUR-NAs and +CPT/CUR-NAs in plasma and NaCl solutions, combination index of +CPT-NA and CUR-NAs, selective cytotoxicity on CT26 and 3T3 cells, hemolytic and RBC aggregation assay. See DOI: 10.1039/d1cc00156f

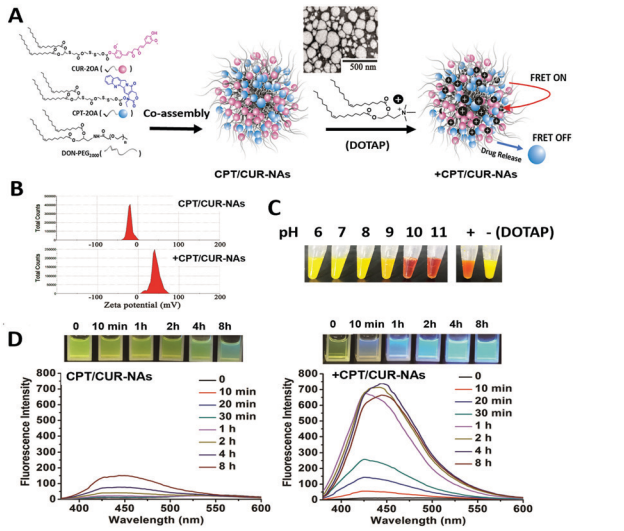


Fig. 1 Schematic illustration of co-assembling FRET CPT/CUR-NAs to monitor CPT release by detecting the recovery of CPT fluorescence (A). Comparative properties of unmodified and cationic CPT/CUR-NAs: zeta potentials (B), appearance (C, CUR solutions at various pH were used as a control), kinetic change of fluorescence and emission spectra in 10 mM DTT (D).

diameters in the range of 124.8–159.1 nm (Fig. S3, ESI†), but showed different zeta potentials (−18.4 mV *vs.* +28.5 mV, Fig. 1B). Interestingly, the unmodified CPT/CUR-NAs show a yellow appearance, whereas +CPT/CUR-NAs had a brownish red appearance (Fig. 1C). This result indicated that cationic NAs had an alkalized interface, because CUR itself was a pH colorimetric indicator with a strong redness-shift under alkaline conditions.[18] Such high pH at the cationic surface might be attributed to the electrostatic adsorption of $OH^-$ ions at the NAs' interface.[19,20]

Due to fluorescence resonance energy transfer (FRET) effects between CPT and CUR, the co-assembly of CPT-SS-2OA and CUR-SS-2OA could result in the complete quenching of CPT fluorescence. The recovery of CPT fluorescence at 426 nm could reflect CPT release (Fig. 1A). This was demonstrated by HPLC analysis (Fig. S4, ESI†), indicating that the cleavage of ETCSS was directly coupled with CPT or CUR release. Therefore, the redox-responsiveness of CPT/CUR-NAs could be readily evaluated by simply detecting the kinetic change of CPT fluorescence, which made them an ideal platform to investigate the effects of various factors on the redox-responsiveness of NAs.[21]

Based on such FRET NAs, we firstly investigated the effect of interfacial cationization on the redox-responsiveness of CPT/CUR-NAs. The dithiothreitol (DTT) was utilized as the model reductive stimulus agent. As shown in Fig. 1D, +CPT/CUR-NAs displayed a rapid CPT fluorescence increase with the maximum level reached after 1 h incubation, which was much faster than that of unmodified CPT/CUR-NAs. Based on the change of CPT fluorescence intensity at 426 nm, +CPT/CUR-NAs exhibited an around 53 fold higher redox-sensitivity than that of unmodified CPT/CUR-NAs. Furthermore, +CPT/CUR-NAs at 0.1 mM DTT could still provide a high fluorescence response, which was comparable to that of unmodified CPT/CUR-NAs at 10 mM DTT (Fig. S5A, ESI†). Such high redox-sensitivity of cationic NAs was probably ascribed to the high interfacial pH of NAs (Fig. 1C). As supporting evidence for this explanation, the fluorescence response of CPT/CUR-NAs was also highly dependent on the pH in bulk solutions (Fig. S6, ESI†). It is worth mentioning that there is nearly no fluorescence increase for +CPT/CUR-NAs after 24 h incubation in 10 mM phosphate buffer (pH 7.4) at 37 °C (Fig. S7, ESI†), indicating that +CPT/CUR-NAs were stable in the absence of reductive agents, despite the high pH at NA-water interfaces.

Considering that the low pH in lysosomal organelles can make the thiol–SS exchange reactions less efficient,[16] the redox-responsiveness of +CPT/CUR-NAs at a lower pH was investigated. As can be seen in Fig. S5B (ESI†), the fluorescence change of CPT/CUR-NAs was greatly decreased at pH of 6.8 and 5.5. By contrast, +CPT/CUR-NAs still displayed an obvious fluorescence response at the low pH of 5.5, which was even 4 folds faster than that of CPT/CUR-NAs at pH 7.4. On the other hand, the cationic NAs were readily able to absorb various anionic ions and proteins in the physiological media, which might potentially interfere with the redox-responsiveness of +CPT/CUR-NAs. To address this concern, the DTT-induced fluorescence change of +CPT/CUR-NAs in plasma and various concentrations of NaCl was also investigated. As shown in Fig. S8 (ESI†), NaCl at the physiologically-relevant concentration (150 mM) did not influence the fluorescence response of +CPT/CUR-NAs. After 30 min incubation in plasma, the positive zeta potential of +CPT/CUR-NAs was inversed from +41.8 mV to −16.4 mV, and the particle size increased from 124.8 nm to 147.7 nm, indicating the extensive adsorption of anionic proteins. Despite this, +CPT/CUR-NAs still exhibited an around 15 fold higher redox-responsivity than that of CPT/CUR-NAs (Fig. S9, ESI†). These results indicated that the interfacial cationization was a robust strategy to increase the redox-responsiveness of CPT/CUR-NAs, which could be even valid at a lower pH or in physiologically relevant media.

We next investigated the effects of proportion of cationic or anionic lipids on the redox-responsiveness of CPT/CUR-NAs (Fig. 2A). It is shown that the particle sizes of +CPT/CUR-NAs were less dependent on the DOTAP proportions (Fig. S10, ESI†), but the zeta potentials of +CPT/CUR-NAs highly depended on the fraction of DOTAP (Fig. 2B). The appearance of CPT/CUR-NAs was changed from yellow into red as the DOTAP increased, indicating the gradual alkalization at the NAs' interface. Accordingly, the increasing rate of fluorescence was positively correlated with the DOTAP proportions, with the maximum fluorescence response at 5% DOTAP (Fig. 2C). Similarly, the redox responsiveness of NAs could also be adjusted by incorporating anionic lipids. It is shown that the zeta potentials of CPT/CUR-NAs became more negative with the increase of anionic lipid of DON-COOH (Fig. 2D, $^1$H-NMR and MS shown in Fig. S11, ESI†). The increase of CPT fluorescence was accordingly lowered, and nearly stopped for NAs containing 20% DON-COOH (Fig. 2E). Based on the fluorescence change before and after 1 h incubation in 10 mM DTT, the maximum difference in the redox-responsiveness of CPT/CUR-NAs can be up to ~1000 folds. These results indicated that the interfacial microenvironment of NAs can modulate their redox-responsiveness by nearly 3 orders of

 

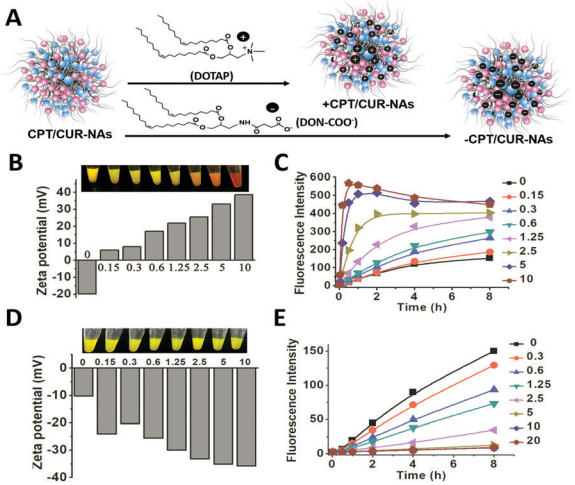


Fig. 2 Schematic illustration of the preparation of cationic and anionic CPT/CUR-NAs (A). Zeta potentials (B and D) and fluorescence response (C and E) of cationic or anionic CPT/CUR-NAs with different weight percentages of DOTAP or DON-COOH.

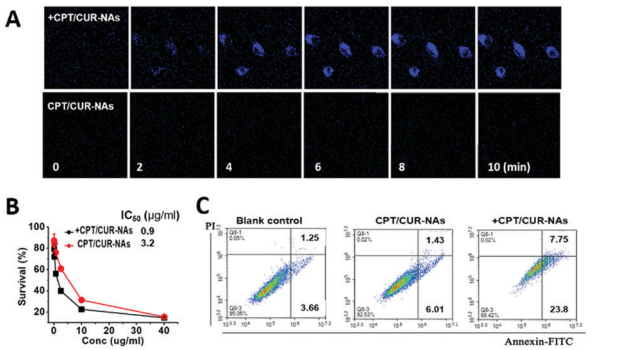


Fig. 3 Real-time visualization of the CPT release in CT26 cells by monitoring the fluorogenic process of CPT/CUR-NAs (B). MTT assay (B) and apoptotic analysis (C) of CT26 cells after the treatment of unmodified and cationic CPT/CUR-NAs.

magnitude in a predictable and finely tunable manner, which provided an opportunity to induce a selective cytotoxicity against tumor cells by utilizing different concentrations of glutathione in cancer cells and normal cells.

The cellular uptake of unmodified and cationic CPT/CUR-NAs was next comparatively investigated in colorectal cancer cells (CT26) using a confocal laser scanning microscope. As shown in Fig. S12 (ESI†), there was nearly no CPT fluorescence (blue) observed for the cells after 0.5 h of incubation with unmodified CPT/CUR-NAs. By contrast, +CPT/CUR-NAs treated cells exhibited a bright CPT fluorescence, which was mainly co-localized with the lysosomal signal (in red). This result indicated that +CPT/CUR-NAs could be rapidly internalized in cells and mainly localized in acid lysosomes. As the CPT release can be self-reported *via* the FRET signal, the recovering of CPT fluorescence suggested that the CPT could be released from cationic NAs. The intracellular CPT release was further detected in a real-time manner by capturing the kinetic change of the fluorescence images. It is shown that the blue CPT fluorescence rapidly appeared within the cationic NA-treated cells within several minutes, indicating a faster CPT release from +CPT/CUR-NAs as compared with that from CPT/CUR-NAs (Fig. 3A). Such faster CPT release from +CPT/CUR-NAs further resulted in a more potent *in vitro* cytotoxicity, with a much lower $IC_{50}$ (CPT equivalent concentration, 0.9 *versus* 3.2 μg $ml^{-1}$, Fig. 3B) and higher apoptosis percentage (31.5% *versus* 7.4%, Fig. 3C) than that of the unmodified NAs. It is worth mentioning that the combination of CPT and CUR in the +CPT/CUR-NAs displayed a synergistic antitumor effect with a low combination index of 0.24–0.4 at the CPT/CUR ratio of 1/2 (Fig. S13, ESI†). On the other hand, a cytotoxicity study was also performed on a normal cell line (mouse fibroblast, 3T3 cells) to evaluate the selective cytotoxicity of NAs between tumor cells and normal cells. As shown in Fig. S14A (ESI†), +CPT/CUR-NAs also induced a higher apoptosis in 3T3 cells, but it also achieved around 2-fold higher selectivity index against CT26 cells than that of CPT/CUR-NAs (Fig. S14B, ESI†). This was probably attributed to the faster intracellular drug release from cationic NAs in CT26 cells (Fig. S14C, ESI†), despite the lower cellular uptake of cationic NAs in CT26 cells as compared with that in 3T3 cells (Fig. S14D, ESI†). These results indicated that the increased redox-responsivity of +CPT/CUR-NAs could not only increase *in vitro* cytotoxicity but also enhance the selective cytotoxicity against tumor cells.

The hemolysis and erythrocyte aggregation of CPT/CUR-NAs and +CPT/CUR-NAs were tested to predict the *in vivo* safety. It is shown that both NAs only caused slight hemolysis at high concentrations, but the cationic NAs resulted in remarkable erythrocyte aggregation as compared to the unmodified NAs (Fig. S15, ESI†). This result indicated that cationic NAs could not be directly intravenously injected, and a "charge reversal" strategy might be required for intravenous injection.[22] However, such redox-ultrasensitive cationic NAs could be directly used for localized cancer therapies, such as *in situ* antitumor vaccine and intravesical therapy of bladder diseases.

Fig. 4 shows the proposed mechanism of the increased redox-responsivity of +CPT/CUR-NAs. Firstly, the directional arrangement of positive charges at the cationic nanoparticle's surface resulted in a high positive surface potential, which further led to the high interfacial pH due to the extensive adsorption of $OH^-$ ions (Fig. 1C). Therefore, thiol species (RSH) approaching the cationic nanoparticle's surface were readily converted into ionized thiolate ($RS^-$). As the chemical reactions of thiol mainly involved the nucleophilic attack of the $RS^-$,[23] the generation of $RS^-$ would facilitate the thiol–SS exchange reactions, thus enhancing the sensitivity of redox-responsive drug release. Furthermore, $RS^-$ was also hypothesized to be electrostatically adsorbed at NAs' surface, which also contributed to greatly increased redox-responsivity. As supporting evidence for this explanation, the interfacial cationization was more effective to increase the redox-responsivity of NAs as compared with that by enhancing the bulk pH of solution (Fig. 1D and Fig. S6, ESI†). Although the pH in the vicinity of the nanoparticle surface has been found to be quite different from the bulk,[19,20,24] to our knowledge, this is the first report that the redox-responsivity of nanocarriers could be adjusted by their interfacial change properties.

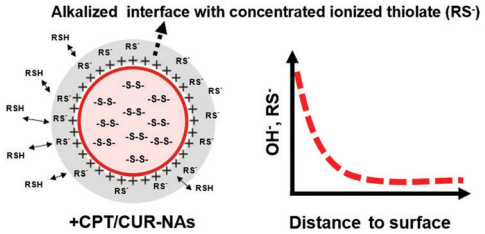


Fig. 4 Proposed mechanism to explain the high redox-sensitivity of +CPT/CUR-NAs. The interfacial cationization induced a high interfacial pH, resulting in the generation and concentration of ionized thiolate ($RS^-$) at the NA–water interface. Such generated $RS^-$ remarkably increased the redox-responsivity of CPT/CUR-NAs by accelerating the thiol–SS exchange reactions.

In conclusion, our results demonstrated that the redox-responsivity of SS-containing nanocarriers could be readily regulated over a broad range (~3 orders of magnitudes) by changing their interfacial charges, which would effectively inspire the design, preparation and characterization of a new generation of stimulus-ultrasensitive therapeutic nanocarriers based on interface designs.

This research was supported by the Foundation for New Teacher Training Program of Chongqing Medical University (YXY20 20XSZ02), and the National Undergraduate Training Program for Innovation and Entrepreneurship (S202013705008, S20201370 5048, and S202013705125).

## Conflicts of interest

There are no conflicts to declare.

## Notes and references

1 R. Cheng, F. Feng, F. Meng, C. Deng, J. Feijen and Z. Zhong, *J. Controlled Release*, 2011, **152**, 2–12.
2 Y. Chi, X. Yin, K. Sun, S. Feng, J. Liu, D. Chen, C. Guo and Z. Wu, *J. Controlled Release*, 2017, **261**, 113–125.
3 J. F. Quinn, M. R. Whittaker and T. P. Davis, *Polym. Chem.*, 2017, **8**, 97–126.
4 H. Wei, R.-X. Zhuo and X.-Z. Zhang, *Prog. Polym. Sci.*, 2013, **38**, 503–535.
5 A. Raza, U. Hayat, T. Rasheed, M. Bilal and H. M. N. Iqbal, *Eur. J. Med. Chem.*, 2018, **157**, 705–715.
6 E. Mirhadi, M. Mashreghi, M. Faal Maleki, S. H. Alavizadeh, L. Arabi, A. Badiee and M. R. Jaafari, *Int. J. Pharm.*, 2020, **589**, 119882.
7 D. Li, R. Zhang, G. Liu, Y. Kang and J. Wu, *Adv. Healthcare Mater.*, 2020, **9**, 2000605.
8 F. Li, Z. Huang, H. T. Chen, L. Yan, J. Li, Y. Su, Q. Zhang, Z. Y. Huang and Y. X. Zheng, *Drug Delivery*, 2019, **26**, 1068–1079.
9 Y. Li, T. Kang, Y. Wu, Y. Chen, J. Zhu and M. Gou, *Chem. Commun.*, 2018, **54**, 1996–1999.
10 C. Luo, J. Sun, B. Sun, D. Liu, L. Miao, T. J. Goodwin, L. Huang and Z. He, *Small*, 2016, **12**, 6353–6362.
11 X. Xia, X. Xiang, F. Huang, Z. Zhang and L. Han, *Chem. Commun.*, 2017, **53**, 13141–13144.
12 B. J. Sun, C. Luo, X. B. Zhang, M. R. Guo, M. C. Sun, H. Yu, Q. Chen, W. Q. Yang, M. L. Wang, S. Y. Zuo, P. Y. Chen, Q. M. Kan, H. T. Zhang, Y. J. Wang, Z. G. He and J. Sun, *Nat. Commun.*, 2019, 10.
13 S. Zuo, B. Sun, Y. Yang, S. Zhou, Y. Zhang, M. Guo, M. Sun, C. Luo, Z. He and J. Sun, *Small*, 2020, **16**, 2005039.
14 A. G. Cheetham, Y.-C. Ou, P. Zhang and H. Cui, *Chem. Commun.*, 2014, **50**, 6039–6042.
15 B. Sun, C. Luo, H. Yu, X. Zhang, Q. Chen, W. Yang, M. Wang, Q. Kan, H. Zhang, Y. Wang, Z. He and J. Sun, *Nano Lett.*, 2018, **18**, 3643–3650.
16 L. Bruelisauer, M. A. Gauthier and J.-C. Leroux, *J. Controlled Release*, 2014, **195**, 147–154.
17 B. A. Kellogg, L. Garrett, Y. Kovtun, K. C. Lai, B. Leece, M. Miller, G. Payne, R. Steeves, K. R. Whiteman, W. Widdison, H. Xie, R. Singh, R. V. J. Chari, J. M. Lambert and R. J. Lutz, *Bioconjugate Chem.*, 2011, **22**, 717–727.
18 J. Liu, H. Wang, P. Wang, M. Guo, S. Jiang, X. Li and S. Jiang, *Food Hydrocolloids*, 2018, **83**, 134–142.
19 D. Singappuli-Arachchige and I. I. Slowing, *J. Chem. Phys.*, 2020, 152.
20 Y. Sarkar, S. Das, A. Ray, S. K. Jewrajka, S. Hirota and P. P. Parui, *Analyst*, 2016, **141**, 2030–2039.
21 Y. Li, J. Zhu, T. Kang, Y. Chen, Y. Liu, Y. Huang, Y. Luo, M. Huang and M. Gou, *Chem. Commun.*, 2018, **54**, 11618–11621.
22 M. Zhang, X. Chen, C. Li and X. Shen, *J. Controlled Release*, 2020, **319**, 46–62.
23 L. Turell, R. Radi and B. Alvarez, *Free Radical Biol. Med.*, 2013, **65**, 244–253.
24 Y. Sarkar, R. Majumder, S. Das, A. Ray and P. P. Parui, *Langmuir*, 2018, **34**, 6271–6284.

 